



Showcasing research from Professor Hiroaki Tada's laboratory, Department of Applied Chemistry, Faculty of Science and Engineering, Kindai University, Osaka, Japan.

Overall water splitting and hydrogen peroxide synthesis by gold nanoparticle-based plasmonic photocatalysts

Gold nanoparticle-based plasmonic photocatalysts can be driven by excitation of the localized surface plasmon resonance. Among them, hot-electron transfer-type photocatalysts have recently attracted interest as promising solar-to-chemical converters owing to the wide spectral response from visible-to-infrared light. This Minireview highlights recent studies on two kinds of artificial photosynthesis - water splitting and H<sub>2</sub>O<sub>2</sub> synthesis from water and oxygen - using hot-electron transfer-type plasmonic photocatalysts with particular emphasis placed on the electrocatalysis of Au nanoparticles.

As featured in:



See Hiroaki Tada, *Nanoscale Adv.*, 2019, 1, 4238.

Cite this: *Nanoscale Adv.*, 2019, 1, 4238

# Overall water splitting and hydrogen peroxide synthesis by gold nanoparticle-based plasmonic photocatalysts

Hiroaki Tada

Plasmonic photocatalysts driven by the localized surface plasmon resonance excitation of gold nanoparticles (Au NPs) can be efficient solar-to-chemical converters due to their wide spectral response. This review article highlights recent studies on plasmonic water splitting and H<sub>2</sub>O<sub>2</sub> synthesis from water and oxygen (O<sub>2</sub>) with a particular emphasis placed on the electrocatalysis of Au NPs. The Introduction (Section 1) points to the importance of the establishment of solar hydrogen and oxygen cycles involving hydrogen (H<sub>2</sub>) and hydrogen peroxide (H<sub>2</sub>O<sub>2</sub>) as the key compound, respectively, for realizing a "sustainable society". Section 2 deals with the basic action mechanisms of Au NP-based plasmonic photocatalysts. Section 3 treats the electrocatalytic activity of Au NPs for the half-reactions involved in the reactions. Section 4 describes recent advances in the plasmonic overall water splitting (4.1) and H<sub>2</sub>O<sub>2</sub> synthesis (4.2). Finally, a summary is presented with the possible development direction in Section 5.

Received 9th July 2019  
Accepted 16th September 2019

DOI: 10.1039/c9na00431a

rsc.li/nanoscale-advances

## 1. Introduction

Hydrogen (H<sub>2</sub>) and hydrogen peroxide (H<sub>2</sub>O<sub>2</sub>) are basic feedstocks in chemical industries, and their use will expand more and more in future due to their environmental benignity. Presently, most H<sub>2</sub> is produced by steam reforming of methane at 700–800 °C using a Ni-based catalyst, while H<sub>2</sub>O<sub>2</sub> is industrially produced by the anthraquinone auto-oxidation involving multiple steps.<sup>1</sup> Both processes consume large amounts of energy and are undesirable from both environmental and economic aspects. Unambiguously, overall water splitting is the ideal process for H<sub>2</sub> production (reaction (1)), while the synthesis of H<sub>2</sub>O<sub>2</sub> from water and oxygen (O<sub>2</sub>) as well as the direct synthesis from H<sub>2</sub> and O<sub>2</sub> (ref. 2) is very beneficial (reaction (2)).



where  $\Delta_r G^0$  is the standard Gibbs energy of reaction.



External energy must be supplied to drive the energetically up-hill reactions. Utilization of thermal energy as the driving force is impossible for both the reactions because only 2% of water is decomposed even at 2000 °C, and H<sub>2</sub>O<sub>2</sub> is vulnerable to heat. In principle, reactions (1) and (2) can be driven by photons

with energy larger than 1.23 eV and 0.54 eV, respectively, under mild conditions. These considerations motivate one to develop photocatalysts for reactions (1) and (2) by effectively utilizing the visible-to-near infrared light abundantly present in sunlight. If such production of H<sub>2</sub> and H<sub>2</sub>O<sub>2</sub> is achieved, input of H<sub>2</sub> into H<sub>2</sub>-O<sub>2</sub> fuel cells and input of H<sub>2</sub>O<sub>2</sub> into one-compartment fuel cells<sup>3–6</sup> and photofuel cells<sup>7</sup> would generate electric energy to complete the solar hydrogen cycle (Scheme 1a) and solar oxygen cycle (Scheme 1b), respectively. So far, many semiconductor



Scheme 1 (a) Solar hydrogen cycle and (b) solar oxygen cycle.

Department of Applied Chemistry, School of Science and Engineering, Kindai University, 3-4-1, Kowakae, Higashi-Osaka, Osaka 577-8502, Japan. E-mail: h-tada@apch.kindai.ac.jp



photocatalysts for water splitting have been intensively studied; however, a band gap larger than  $\sim 2.5$  eV is usually necessary<sup>8</sup> because of the large overpotentials for water splitting, particularly the water oxidation reaction (WOR).<sup>9</sup> The same is true for the synthesis of H<sub>2</sub>O<sub>2</sub> from water and O<sub>2</sub> by semiconductor photocatalysts including graphitic carbon nitride (g-C<sub>3</sub>N<sub>4</sub>)<sup>10–13</sup> and bismuth vanadate.<sup>14</sup> On the other hand, the research on Au NP-based plasmonic photocatalysts with strong and broad absorption in the visible-to-near infrared region due to the localized surface plasmon resonance (LSPR) is rapidly progressing.<sup>15–22</sup> The great advantage of plasmonic photocatalysts over semiconductor ones is the availability of “hot carriers” generated by the absorption of such low-energy-photons for chemical reactions,<sup>15,17,18,21</sup> which is a prerequisite for achieving high solar-to-chemical conversion efficiency.

This article reviews recent advances in the plasmonic overall water splitting and H<sub>2</sub>O<sub>2</sub> synthesis from water and O<sub>2</sub>. This field is still in its infancy, but I believe that this article would contribute to the acceleration and future development in the very important and fascinating topics.

## 2. Action mechanisms of plasmonic photocatalysts

Plasmonic photocatalysts can be categorized into the hot-electron transfer (HET)-type<sup>23,24</sup> and the local electric field-enhanced (LEFE)-type<sup>25–28</sup> or the plasmon-resonant energy-transfer-type.<sup>29</sup> Here the basic action mechanisms of the HET- and LEFE-type plasmonic photocatalysts are explained for the typical heterostructures of Au NP-loaded semiconductors (Au/semiconductor) and Au NP-incorporated semiconductors (Au@semiconductor) including Au NP (core)–semiconductor (shell) nanostructures, respectively.

### 2.1 Hot-electron transfer mechanism

The excitation of the LSPR of Au NP generates excited carriers referred to as “hot carriers” having sufficient energy to drive chemical reactions through the non-radiative decay process or the Landau damping with an efficiency of  $\phi_{\text{HCG}}$ .<sup>21</sup> In the HET-type (Fig. 1), the hot electrons are transferred to the conduction band (CB) of a semiconductor.<sup>23,24</sup> The CB-electrons cause a reduction reaction on the semiconductor surface, while an oxidation reaction is induced by the holes left in Au NPs. In this case, solar-to-chemical conversion efficiency ( $\phi_{\text{STC}}$ ) can be provided by multiplication of the efficiencies of light harvesting



Fig. 1 Hot electron transfer mechanism.

by the plasmonic metal (LHE<sub>PM</sub>),  $\phi_{\text{HCG}}$ , hot-electron injection from the plasmonic metal to semiconductor ( $\phi_{\text{INJ(Au} \rightarrow \text{SEM})}$ ), charge separation ( $\phi_{\text{CS}}$ ), and redox reaction efficiency ( $\phi_{\text{redox}}$ ) (eqn (3)).

$$\phi_{\text{STC}}(\text{HET}) = \text{LHE}_{\text{PM}} \times \phi_{\text{HCG}} \times \phi_{\text{INJ(Au} \rightarrow \text{SEM})} \times \phi_{\text{CS}} \times \phi_{\text{redox}} \quad (3)$$

### 2.2 Local electromagnetic field-enhanced mechanism

On the other hand, in the LEFE-type (Fig. 2), redox reactions are caused by the band gap excitation of a semiconductor. In this case, the active optical antenna effect of Au NPs enhances the LHE of the semiconductor.<sup>30</sup> The local electric field enhancement of Au NPs increases the rate of electron–hole generation in the semiconductor, further promoting the charge separation.<sup>26,31</sup> Thus, the  $\phi_{\text{STC}}$  is expressed by multiplication of the efficiencies of light harvesting by Au@semiconductor (LHE<sub>Au@SEM</sub>), carrier generation ( $\phi_{\text{CG}}$ ),  $\phi_{\text{CS}}$ , and  $\phi_{\text{redox}}$  (eqn (4)).

$$\phi_{\text{STC}}(\text{LEFE}) = \text{LHE}_{\text{Au@SEM}} \times \phi_{\text{CG}} \times \phi_{\text{CS}} \times \phi_{\text{redox}} \quad (4)$$

Ag NPs possess a LEFE factor much greater than that of Au NPs, and for example, Ag NP-incorporated AgX (X = Cl, Br, and I) can be a promising plasmonic photocatalyst.<sup>32</sup> Excellent review papers on Ag-based plasmonic photocatalysts have recently been published,<sup>33,34</sup> however, the photocatalytic reaction is almost limited to the decomposition of organic dyes. It should also be stressed that most features of plasmonic photocatalysts or the wide spectral response can be obtained only for the HET-type. Also, in both types, the reduction in the overpotentials for the redox reactions is pivotal to enhance the photocatalytic activity.

### 2.3 Photothermal and light-scattering effects

As the secondary effects, photothermal conversion and light scattering can enhance the activity of plasmonic photocatalysts. Generally, radiative damping is the dominant decay mechanism for large Au NPs larger than 50 nm for dipolar plasmon resonances, while nonradiative damping is the dominant decay mechanism for small Au NPs.<sup>35</sup>

Strong light absorption due to the LSPR of Au NPs followed by nonradiative energy dissipation causes a rise in temperature

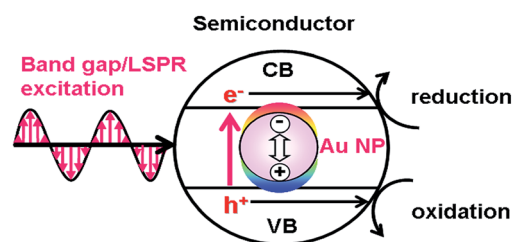


Fig. 2 Local electromagnetic field-enhanced mechanism.



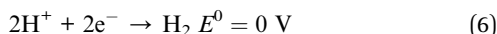
of the surroundings.<sup>36</sup> Particularly, under high-power irradiation, this photothermal effect may boost  $\phi_{\text{STC}}$  for the HET-type and LEFE-type plasmonic photocatalysts through the increases in  $\phi_{\text{redox}}$  shown in eqn (3) and (4). The LSPR extinction band for plasmonic metal NPs consists of the contributions from light absorption and scattering. When the size of Au particles exceeds 50 nm, light scattering becomes dominant.<sup>37</sup> In the LEFE-type plasmonic photocatalysts, light scattering effectively increases to enhance the rate of photogenerated charge carriers in the semiconductor.<sup>38</sup> Thus, the light-scattering effect can boost the  $\phi_{\text{STC}}$  through the increase in LHE shown in eqn (4). However, the light scattering effect would be usually negligible because the particle size of Au NPs used in most studies on plasmonic photocatalysts is significantly smaller than 50 nm.

### 3. Electrocatalytic activity of gold nanoparticles

The oxidation half-reaction common in overall water splitting and  $\text{H}_2\text{O}_2$  synthesis from water and  $\text{O}_2$  is the WOR (reaction in the reverse direction of reaction (5)), where  $E^0$  is the standard electrode potential with respect to the standard hydrogen electrode (SHE).



On the other hand, the reduction half-reactions in the former and latter are the hydrogen evolution reaction (HER, reaction (6)) and the two-electron oxygen reduction reaction (ORR) (reaction (7)), respectively. The key aspect in  $\text{H}_2\text{O}_2$  synthesis is to restrict the four-electron ORR (reaction (5)), which is thermodynamically more favored than the two-electron ORR. The selectivity for electrochemical  $\text{H}_2\text{O}_2$  formation can be quantitatively determined using the rotating ring disk technique.<sup>39</sup>



The electrocatalytic activities of Au NPs for these reactions are described below.

#### 3.1 Electrocatalytic activity for the water oxidation reaction

Misawa and co-workers first showed that the WOR occurs on an Au nanorod-loaded  $\text{TiO}_2$  electrode under illumination of visible and even near infrared light.<sup>40</sup> We studied the electrocatalytic activity of Au/ $\text{TiO}_2$  films coated on a fluorine-doped tin oxide photoanode (Au/ $\text{TiO}_2$ /FTO) for the WOR in a three-electrode photoelectrochemical (PEC) cell with the structure of photoanode|0.1 mol  $\text{dm}^{-3}$   $\text{NaClO}_4$  aqueous solution|Ag/AgCl (reference electrode)|glassy carbon (cathode) under illumination of simulated sunlight (AM 1.5 one sun,  $\lambda > 430 \text{ nm}$ ).<sup>41</sup> Fig. 3a shows the time courses for  $\text{O}_2$  generation in aqueous solution.  $\text{TiO}_2$ /FTO is inactive for the WOR under these conditions. In the Au/ $\text{TiO}_2$ /FTO system,  $\text{O}_2$  concentration increases in proportion to irradiation time. Also, the rate of  $\text{O}_2$  generation increases with a decrease in Au particle size ( $d_{\text{Au}}$ ). García and co-workers also reported the



Fig. 3 (a) Time courses for the rate of  $\text{O}_2$  generation. (b) IPCE action spectrum for the photoelectrochemical WOR of the Au/ $\text{TiO}_2$ /FTO photoelectrodes with the absorption spectrum for comparison. Figure (a) is taken from ref. 41.

same trend in an Au/ $\text{TiO}_2$  particulate system.<sup>42</sup> Fig. 3b shows the action spectrum of the incident photon-to-current efficiency (IPCE) for the Au/ $\text{TiO}_2$ /FTO photoanode cell. Surprisingly, the IPCE rises at excitation energy ( $\hbar\omega$ )  $\approx 1.5 \text{ eV}$ . As the wavelength of incident light shortens, the IPCE increases with a peak near the LSPR peak. A similar action spectrum was reported for the WOR in a PEC cell employing Au/ $\text{SrTiO}_3$  as the photoanode.<sup>43</sup> Also, the electrocatalytic activity of Au/ $\text{TiO}_2$  for the WOR can be dramatically enhanced by the formation of a Pb shell on the Au NPs.<sup>44</sup>

Scheme 2 shows the energy diagram of the Au/ $\text{TiO}_2$  plasmonic anode with the intraband transition *via* the surface plasmon decay.<sup>45</sup> The excitation by photons with  $\hbar\omega = 1.5 \text{ eV}$  promotes the electrons with energy below the Fermi energy ( $E_{\text{F}}$ ) to high energy levels within the 6sp-band. The hot electrons are injected into the CB of  $\text{TiO}_2$ , while the hot holes oxidize water. In this manner, the rise in the IPCE at  $\hbar\omega \geq 1.5 \text{ eV}$  can be explained by the intraband-transition mechanism, and in this scheme, the WOR by the hot holes would determine the rate of the reaction.

#### 3.2 Electrocatalytic activity for the hydrogen evolution reaction

The electrocatalytic activity of bulk-state metal electrodes for the HER can be correlated to the M–H bond energy.<sup>46</sup> A clear



Scheme 2 Energy diagram of the Au/ $\text{TiO}_2$  plasmonic electrode with the density of states of  $\text{TiO}_2$  and energy distribution of the hot carriers in Au NPs with the intraband transition *via* the surface plasmon decay.



volcano-shaped curve in the plots of electrocatalytic activity for the HER *vs.* Gibbs energy of metal–H bond formation indicates that the group of metals with moderate M–H bond energy have high levels of activity for the HER. Among metal electrodes, Au possesses a high electrocatalytic activity for the HER following some rare metals (Pt, Re, Rh, and Ir). Then, to evaluate the electrocatalytic activity of Au NPs, the Au/TiO<sub>2</sub>-photocatalyzed H<sub>2</sub> generation from ethanol aqueous solution was carried out under UV-light irradiation in the absence of O<sub>2</sub>. UV-light irradiation of Au/TiO<sub>2</sub> excites the electrons in the valence band (VB) of TiO<sub>2</sub> to the CB (eqn (8)). The CB-electrons in TiO<sub>2</sub> are effectively transferred to Au NPs with a large work function to be accumulated in them (eqn (9)).<sup>47</sup> The VB-holes in TiO<sub>2</sub> easily oxidize ethanol to yield acetaldehyde and protons (eqn (10)). On the other hand, the electrons accumulated in Au NPs reduce water to H<sub>2</sub> (eqn (11)). Accordingly, the photocatalytic activity can be a good indicator of the electrocatalytic activity of Au NPs for the HER.



Idriss and co-workers reported Au/TiO<sub>2</sub>-photocatalyzed H<sub>2</sub> generation from an aqueous solution of ethanol.<sup>48</sup> The authors showed that UV-light irradiation of Au/anatase TiO<sub>2</sub> and Au/rutile TiO<sub>2</sub> yields H<sub>2</sub>, while each unmodified TiO<sub>2</sub> is inactive. Interestingly, the activity of Au/anatase TiO<sub>2</sub> is significantly higher than that of Au/rutile TiO<sub>2</sub> at the same Au loading, further exceeding the activity of Pt/TiO<sub>2</sub>.

### 3.3 Electrocatalytic activity for the oxygen reduction reaction

In bulk-state electrodes, the two-electron ORR preferentially proceeds on Au, while the four-electron ORR occurs on Pt.<sup>49</sup> The photocatalytic activity of metal NP-loaded TiO<sub>2</sub> (M/TiO<sub>2</sub>, M = Au and Pt) for the ORR was carried out in aerated ethanol aqueous solution under UV-light irradiation (M/TiO<sub>2</sub>, M = Au and Pt).<sup>50</sup> In this case, the electrons in metal NPs can be used for the two-electron and/or four-electron ORR (reactions (12) and (13)), and the photocatalytic activity can be a good indicator of the electrocatalytic activity of metal NPs for the ORR.

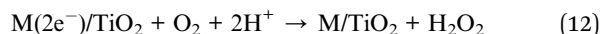


Fig. 4a shows the comparison of the photocatalytic activity of TiO<sub>2</sub>, Au/TiO<sub>2</sub>, and Pt/TiO<sub>2</sub> for the two-electron ORR. In the TiO<sub>2</sub> system, only micromolar H<sub>2</sub>O<sub>2</sub> is generated as previously reported.<sup>51–53</sup> Loading Pt NPs on TiO<sub>2</sub> increases the saturated H<sub>2</sub>O<sub>2</sub> concentration to ~1 mmol dm<sup>-3</sup>. Strikingly, Au/TiO<sub>2</sub> exhibits much higher activity than Pt/TiO<sub>2</sub>, and the H<sub>2</sub>O<sub>2</sub> concentration reaches ~6 mmol dm<sup>-3</sup> at irradiation time = 24



Fig. 4 Time courses for the M(Au and Pt)/TiO<sub>2</sub>-photocatalyzed ORR to H<sub>2</sub>O<sub>2</sub> under UV-light irradiation ( $\lambda > 300 \text{ nm}$ , light intensity  $I_{290-390 \text{ nm}} = 3 \text{ mW cm}^{-2}$ ) and unmodified TiO<sub>2</sub> system for comparison. (b) Adsorption energy change with the M<sub>28</sub>/TiO<sub>2</sub>-photocatalyzed two-electron ORR (M = Au and Pt. Figure (b) is taken from ref. 54.

h. To gain information about the origin of the great difference of the activity, density functional theory (DFT) simulations were performed for model systems (Au<sub>28</sub>/(TiO<sub>2</sub>)<sub>32</sub> and Pt<sub>28</sub>/(TiO<sub>2</sub>)<sub>32</sub>).<sup>54</sup> Fig. 4b shows the comparison of the adsorption energy of the sequentially reduced O<sub>2</sub> species and the optimized structures. The one-electron ORR to OOH<sub>(ad)</sub> is an energetically large downhill process, and the structure is the same in each system. In the two-electron ORR, the OOH<sub>(ad)</sub> can be reduced to HOOH in the Au<sub>28</sub>/(TiO<sub>2</sub>)<sub>32</sub> system, whereas H<sub>2</sub>O<sub>(ad)</sub> and O<sub>(ad)</sub> are produced with the O–O bond cleavage in the Pt<sub>28</sub>/(TiO<sub>2</sub>)<sub>32</sub> system. In the electrode systems, the selectivity for electrochemical H<sub>2</sub>O<sub>2</sub> formation was reported to be 6.3% for Au/TiO<sub>2</sub> and <0.1% for Pt/TiO<sub>2</sub>.<sup>10</sup> These experimental and theoretical calculation results indicate that the Au NP catalyst is a good electrocatalyst for the two-electron ORR, while Pt NPs accelerate the four-electron ORR.

## 4. Photocatalytic reactions

Usually, the photocatalytic activity can be evaluated using the external quantum yield ( $\phi_{\text{ex}}$ ) defined by eqn (1).

$$\phi_{\text{ex}} = \left\{ n \times \left( \frac{\text{number of product molecules}}{\text{number of incident photons}} \right) \right\} \quad (14)$$

where  $n = 2$  for the HER (product = H<sub>2</sub>) and the 2-electron ORR (product = H<sub>2</sub>O<sub>2</sub>), and  $n = 4$  for the WOR (O<sub>2</sub>).

### 4.1 Overall water splitting

Moskovits and co-workers were the first to show plasmonic overall water splitting using TiO<sub>2</sub>-capped Au nanorods with Pt as the hydrogen evolution catalyst on TiO<sub>2</sub> and a Co-based oxygen evolution catalyst on Au ( $\phi_{\text{ex}} = \sim 0.1\%$ ).<sup>55</sup> The Au/TiO<sub>2</sub>-NiO<sub>x</sub> plasmonic photocatalyst has also been reported to be capable of splitting water with  $\phi_{\text{ex}} = 0.013\%$  at  $\hbar\omega = 2.1 \text{ eV}$ .<sup>56</sup> As shown in Scheme 2, the low CB minimum of TiO<sub>2</sub> ( $E_{\text{CBM}} = -4.1 \text{ eV}$  for rutile TiO<sub>2</sub> and  $-3.9 \text{ eV}$  for anatase TiO<sub>2</sub> at pH 7 *vs.* vacuum level) which is insufficient for the HER ( $E_{\text{CBM}} = -4.02 \text{ eV}$  at pH 7) is mainly responsible for the limited efficiencies. On



the other hand, CdS possesses a much higher CB minimum ( $E_{\text{CBM}} = -3.28$  eV).<sup>57</sup> Unique asymmetrical nano hybrids referred to as half-cut Au (core) and CdS (shell) nanoeggs without and with a heteroepitaxial junction (HC-Au@CdS and HC-Au@#CdS) were synthesized using a modified photo-deposition technique.<sup>58</sup> Water splitting experiments were carried out under irradiation of red-light.<sup>59</sup> Fig. 5a shows the comparison of the photocatalytic activity of the nano hybrids and the single components. In this case, the Au particle size was fixed at  $\sim 5.5$  nm. Au and CdS are almost inactive, but the physical mixture shows a low activity. Interestingly, non-heteroepitaxial junction HC-Au@CdS has much higher activity, which further increases more than twice in the heteroepitaxial junction sample. As shown in Fig. 5b, the photocatalytic activity increases by about one-order of magnitude with an increase in Au particle size from 5.5 nm to 12.1 nm, and  $\phi_{\text{ex}} = 0.24\%$  at  $\hbar\omega = 1.9$  eV has been achieved. Further, even after three repetitions of the 3 day-reaction, no decay in the activity is observed with the continuous stoichiometric generation of  $\text{H}_2$  and  $\text{O}_2$ .

Scheme 3 illustrates the basic reaction scheme of water splitting by the HC-Au@#CdS plasmonic photocatalyst. HC-Au@#CdS efficiently absorbs sunlight. The hot-electrons generated by the LSPR excitation can be effectively injected into the CB of CdS<sup>60–62</sup> through the large area and high-quality junction.<sup>59</sup> The high-energy electrons in the CB of CdS enable a smooth HER, while the hot holes left in Au NPs oxidize water with the aid of the electrocatalytic activity for the WOR.<sup>63</sup> Importantly, selective excitation of the Au NP-LSPR suppresses the photodissolution of CdS,<sup>64</sup> so far hampering its use as a water splitting photocatalyst.

Tan and co-workers have recently prepared a Pt NP-loaded  $\text{TiO}_2$  hierarchical nano-architecture (Pt/ $\text{TiO}_2$ -HA), showing that it has a high level of visible-light activity for overall water splitting ( $\phi_{\text{ex}} = 0.23\%$  at  $\hbar\omega = 2.25$  eV).<sup>65</sup> The authors postulated the HET mechanism described in Section 2.1 for the Pt/ $\text{TiO}_2$ -HA-photocatalyzed water splitting.

## 4.2 Hydrogen peroxide synthesis

Au/ $\text{TiO}_2$  plasmonic photocatalysts have been applied to various important oxidations.<sup>66</sup> This is probably because the

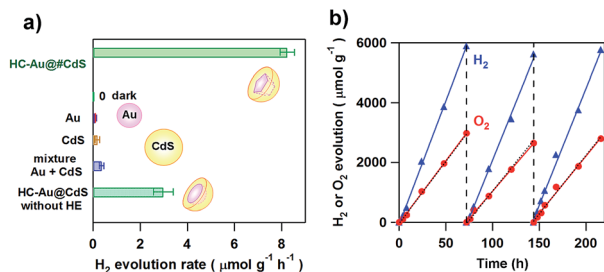


Fig. 5 (a) The comparison of the  $\text{H}_2$  evolution rate for HC-Au( $d_{\text{Au}} = 5.5$  nm)@#CdS( $\text{ICdS} = 1.9$  nm), Au colloid, CdS, and a mixture of Au and CdS under red-light illumination ( $\lambda_{\text{ex}} = 640$  nm) or dark conditions. (b) Repeated water splitting by HC-Au( $d_{\text{Au}} = 12.1$  nm)@#CdS( $\text{ICdS} = 2.1$  nm) under red-light illumination. Figures are taken from ref. 59.



Scheme 3 Schematic representation of water splitting by the HC-Au@#CdS/ $\text{TiO}_2$  plasmonic photocatalyst.

electrocatalytic activity of Au NPs for the reduction reaction cannot be utilized in the usual HET-type Au/ $\text{TiO}_2$  plasmonic photocatalyst, where Au and  $\text{TiO}_2$  act as oxidation and reduction sites, respectively (Fig. 1). We have shown that visible-light irradiation of small- ( $d_{\text{Au}} \approx 2$  nm) and large- ( $d_{\text{Au}} \approx 10$  nm) Au NP-loaded  $\text{TiO}_2$  referred to as bimodal (BM)-Au/ $\text{TiO}_2$  induces the interfacial electron transfer from small Au NPs to large Au NPs through the CB of  $\text{TiO}_2$ .<sup>67</sup> This phenomenon was rationalized in terms of the entropic driving force for the interfacial electron transfer.<sup>33</sup> Fig. 6a shows the time courses for BM-Au/ $\text{TiO}_2$ -photocatalyzed  $\text{H}_2\text{O}_2$  generation from aerated water in the absence and presence of ethanol under visible-light irradiation.<sup>68</sup> Even without ethanol,  $\sim 40 \mu\text{mol dm}^{-3}$   $\text{H}_2\text{O}_2$  is generated at irradiation time = 40 min. Fig. 6b shows the comparison of the photocatalytic activity of various catalysts for  $\text{H}_2\text{O}_2$  generation from aerated aqueous ethanol solution. BM-Au/ $\text{TiO}_2$  exhibits much higher activity than small-Au/ $\text{TiO}_2$  and large-Au/ $\text{TiO}_2$ .

It is known that  $\text{H}_2\text{O}_2$  strongly adsorbs on  $\text{TiO}_2$  to form a surface complex (eqn (15)). The surface complex undergoes reductive decomposition by the CB-electrons in  $\text{TiO}_2$  (eqn (16)).<sup>69</sup> Then, it is also important to suppress this degradation

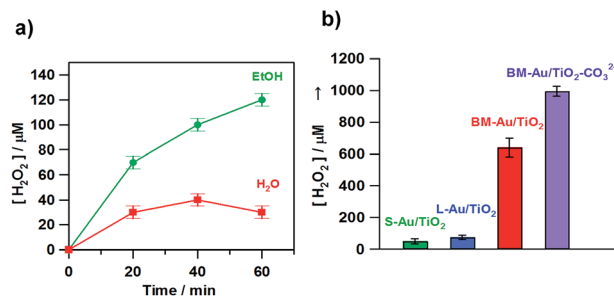


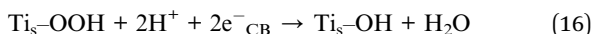
Fig. 6 (a) Time courses for the BM-Au/ $\text{TiO}_2$ -photocatalyzed  $\text{H}_2\text{O}_2$  generation in the absence (red) and presence of 4%  $\text{C}_2\text{H}_5\text{OH}$  (green) under irradiation of visible-light ( $\lambda_{\text{ex}} > 430$  nm, light intensity integrated from 420 to 485 nm =  $4.0 \text{ mW cm}^{-2}$ ) at 298 K. (b) Photocatalytic activity of S-Au/ $\text{TiO}_2$ , L-Au/ $\text{TiO}_2$ , BM-Au/ $\text{TiO}_2$ , and BM-Au/ $\text{TiO}_2$ - $\text{CO}_3^{2-}$  for the reduction of  $\text{O}_2$  to  $\text{H}_2\text{O}_2$  in an aqueous solution containing 4%  $\text{HCOOH}$  (pH 1.7) in the dark and under irradiation of visible-light ( $\lambda_{\text{ex}} > 430$  nm, light intensity integrated from 420 to 485 nm =  $4.0 \text{ mW cm}^{-2}$ ) at 298 K. Figures are taken from ref. 68.



pathway to increase the yield of  $\text{H}_2\text{O}_2$ . An effective way is the surface-fluorination of  $\text{TiO}_2$  (ref. 70 and 71) enabling the production of  $\text{H}_2\text{O}_2$  at a millimolar level under UV-light irradiation.<sup>72</sup>



where the subscript *s* denotes the surface atom.

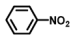
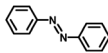
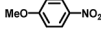
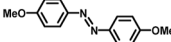

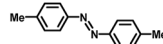
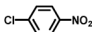
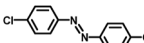
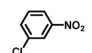
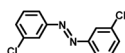


Then, the effect of the surface modification of BM-Au/TiO<sub>2</sub> with carbonate ions (BM-Au/TiO<sub>2</sub>-CO<sub>3</sub><sup>2-</sup>) on the photocatalytic activity was examined. As shown in Fig. 6b, the surface modification drastically increases the photocatalytic activity, and the  $\phi_{\text{ex}}$  reached 5.4% at  $\hbar\omega = 2.3$  eV. In the  $\text{H}_2\text{O}_2$  synthesis from water and  $\text{O}_2$  using semiconductor photocatalysts, a  $\phi_{\text{ex}}$  value of 0.24% at  $\hbar\omega = 2.95$  eV was reported for Au/BiVO<sub>4</sub>.<sup>14</sup> Importantly, Shiraishi and co-workers have found that g-C<sub>3</sub>N<sub>4</sub> possesses an extremely high selectivity of ~90% for electrochemical  $\text{H}_2\text{O}_2$  formation,<sup>10</sup> and the efficiency of photocatalytic  $\text{H}_2\text{O}_2$  synthesis was greatly improved by using it as the photocatalyst ( $\phi_{\text{ex}} = 2.6\%$  at  $\hbar\omega = 2.95$  eV).<sup>73</sup> In a holey defective g-C<sub>3</sub>N<sub>4</sub> photocatalytic system, an extremely high  $\phi_{\text{ex}}$  value of ~16% was achieved in the presence of 2-propanol as an electron donor at  $\hbar\omega = 3.26$  eV.<sup>13</sup>

The high photocatalytic activity of BM-Au/TiO<sub>2</sub> for  $\text{H}_2\text{O}_2$  synthesis from water and  $\text{O}_2$  can be rationalized as follows (Scheme 4). Visible-light irradiation of BM-Au/TiO<sub>2</sub> gives rise to the net electron transport from small Au NPs to large Au NPs, accumulating electrons and holes in large and small Au NPs, respectively. As a result, water is oxidized on small Au NPs (Fig. 3a), while the two-electron ORR occurs on large Au NPs. Eventually, the high photocatalytic activity of BM-Au/TiO<sub>2</sub> for  $\text{H}_2\text{O}_2$  synthesis can stem from the effective charge separation through the interfacial electron transfer from small Au NPs to large Au NPs, the former's excellent electrocatalytic activity for the WOR, and the low catalytic activity of the small and large Au NPs for  $\text{H}_2\text{O}_2$  decomposition.<sup>50</sup> Further, the surface modification with CO<sub>3</sub><sup>2-</sup> ions of BM-Au/TiO<sub>2</sub> is effective in suppressing the reductive decomposition of  $\text{H}_2\text{O}_2$  to increase its yield.

From a viewpoint of organic synthesis, BM-Au/TiO<sub>2</sub> has also paved a way for the application of plasmonic photocatalysts in

Table 1 BM-Au/TiO<sub>2</sub> photocatalyzed reduction of nitrobenzenes<sup>a</sup>

Substrate	Product	Time	Conversion	Selectivity
		12 h	95%	>99%
		24 h	>99%	>99%
		20 h	98%	>99%
		24 h	>99%	>99%
		12 h	>99%	>99%

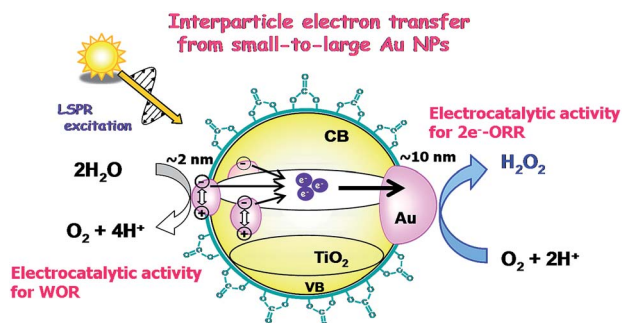
<sup>a</sup> Reaction conditions: BM-Au/TiO<sub>2</sub> 10 mg, nitrobenzene (10 mM) solution (10 mL, 2-propanol) with KOH (10 mM), visible-light ( $\lambda_{\text{ex}} > 430$  nm, 10 mW cm<sup>-2</sup>) irradiation at 25 °C under anaerobic conditions. The table is taken from ref. 67.

reductive chemical transformations. As an example, Table 1 summarizes the BM-Au/TiO<sub>2</sub>-photocatalyzed reduction of nitrobenzene and its derivatives.<sup>67</sup> BM-Au/TiO<sub>2</sub> exhibits a high level of visible-light activity for the one-step synthesis of azobenzenes from nitrobenzenes at 25 °C with a high yield of >95% and selectivity > 99%, whereas unimodal Au/TiO<sub>2</sub> is photocatalytically inactive.

## 5. Summary and perspectives

$\text{H}_2$  and  $\text{H}_2\text{O}_2$  are not only basic chemical feedstocks but also the key compounds for the energy cycles. A big challenge in chemistry is the development of highly active photocatalysts for the overall water splitting and  $\text{H}_2\text{O}_2$  synthesis from water and  $\text{O}_2$ . The HET-type Au NP-based plasmonic photocatalysts can generate "hot carriers" with potential to drive the energetically uphill reactions through the excitation by low-energy photons which the usual semiconductor photocatalysts cannot utilize. The overall water splitting and  $\text{H}_2\text{O}_2$  synthesis comprise the half-reactions of the WOR, HER, and two-electron ORR. Au NPs possess high levels of electrocatalytic activities for these reactions strongly depending on the size, shape, and composition.<sup>74</sup> Consequently, the Au NP-based HET-type plasmonic photocatalyst can be a very promising solar-to-chemical converter.

However, there is plenty of room for the enhancement of the photocatalytic activity by the judicious selection of semiconductors and the optimization of Au NPs corresponding to the targeted reaction. First, the information about the influence of the band structure of semiconductors on the activity is a prerequisite for the rational design of plasmonic photocatalysts. Second, the bimetalization of Au NPs has great potential for improving the photocatalytic activity, while the effects of Au NP-size and shape on the activity have been reviewed.<sup>22</sup> Alloying of Au NPs with Pd<sup>75</sup> and Pt,<sup>76</sup> and Pd/Pt-shell formation on the surface of Au NPs<sup>77</sup> have been reported to boost the activity of the Au/TiO<sub>2</sub> plasmonic photocatalyst for the HER from water containing methanol as a sacrificial electron



Scheme 4 Schematic representation of  $\text{H}_2\text{O}_2$  synthesis from water and  $\text{O}_2$  by the BM-Au/TiO<sub>2</sub> plasmonic photocatalyst.



donor. These effects would partly result from the excellent electrocatalytic activity of Pt and Pd for the HER. Third, as a common subject in heteronanostructured photocatalysts, the importance of devising a general mechanism for enhancing the charge separation between the components should also be stressed. An effective approach to achieve this is the formation of an atomically commensurate heteroepitaxial junction.<sup>59,78,79</sup> In addition, the construction of multi-component plasmonic photocatalysts is also very promising. Recently, three-component plasmonic photocatalysts such as Au and Pt NP-codeposited TiO<sub>2</sub> (ref. 80) and Au/TiO<sub>2</sub>-graphitic carbon nitride (g-C<sub>3</sub>N<sub>4</sub>)<sup>81</sup> have been reported to show much higher photocatalytic activity than Au/TiO<sub>2</sub> for the HER from methanol aqueous solution. The effective charge separation through the interfacial electron transfer from Au NPs to Pt NPs in the former system, and from g-C<sub>3</sub>N<sub>4</sub> to TiO<sub>2</sub> in the latter system would be responsible for the high photocatalytic activities. Meanwhile, the research on the catalysis of supported Au NPs for various reactions is intensively and constantly continued.<sup>82</sup> I anticipate that the combination of the research on the catalysis of Au NPs and Au NP-based plasmonic photocatalysts can effect further development of various “green” processes for solar-to-chemical transformations.

## Conflicts of interest

There are no conflicts to declare.

## Acknowledgements

The author expresses sincere gratitude to Emeritus Professor Dr Hisayoshi Kobayashi (Kyoto Institute of Technology), Dr Musashi Fujishima, Dr Shin-ichi Naya, Ms Miwako Teranishi, T. Onishi, S. Kawano, and Y. Motokawa (Kindai University). This work was supported by the Ministry of Education, Science and Culture, Grant-in-Aid for Scientific Research (C) no. 15K05654, and MEXT-Supported Program for the Strategic Research Foundation at Private Universities.

## Notes and references

- J. M. Campos-Martin, G. Blanco-Brieva and J. L. G. Fierro, *Angew. Chem., Int. Ed.*, 2006, **45**, 6962.
- J. K. Edwards, B. Solsona, E. Ntainjua, N. A. F. Carley, A. A. Herzing, C. J. Kiely and G. J. Hutchings, *Science*, 2009, **323**, 1037.
- S.-i. Yamazaki, Z. Siroma, H. Senoh, T. Iori, N. Fujiwara and K. Yasuda, *J. Power Sources*, 2008, **178**, 20.
- Y. Yamada, S. Yoshida, T. Honda and S. Fukuzumi, *Energy Environ. Sci.*, 2011, **4**, 2822.
- A. M. Shaegh, N.-T. Nguyen, S. M. M. Ehteshami and S. H. Chan, *Energy Environ. Sci.*, 2012, **5**, 8225.
- K. Mase, M. Yoneda, Y. Yamada and S. Fukuzumi, *Nat. Commun.*, 2016, **7**, 11470.
- T. Onishi, M. Fujishima and H. Tada, *ACS Omega*, 2018, **3**, 12099.
- A. Kudo and Y. Miseki, *Chem. Soc. Rev.*, 2009, **38**, 253.
- D. M. Fabian, S. Hu, N. Singh, F. A. Houle, T. Hisatomi, K. Domen, F. E. Osterloh and S. Ardo, *Energy Environ. Sci.*, 2015, **8**, 2825.
- Y. Shiraishi, S. Kanazawa, Y. Sugano, D. Tsukamoto, H. Sakamoto, S. Ichikawa and T. Hirai, *ACS Catal.*, 2014, **4**, 774.
- L. Yang, G. Dong, D. L. Jacobs, Y. Wang, L. Zang and C. Wang, *J. Catal.*, 2017, **352**, 274.
- Y. Peng, L. Wang, Y. Liu, H. Chen, J. Lei and J. Zhang, *Eur. J. Inorg. Chem.*, 2017, 4976.
- L. Shi, L. Yang, W. Zhou, Y. Liu, L. Yin, X. Hai, H. Song and J. Ye, *Small*, 2018, **14**, 1703142.
- H. Hirakawa, S. Shiota, Y. Shiraishi, H. Sakamoto, S. Ichikawa and T. Hirai, *ACS Catal.*, 2016, **6**, 4976.
- K. Ueno and H. Misawa, *J. Photochem. Photobiol., C*, 2013, **15**, 31.
- X. Lang, X. Chen and J. Zhao, *Chem. Soc. Rev.*, 2014, **43**, 473; C. Wang and D. Astruc, *Chem. Soc. Rev.*, 2014, **43**, 7188.
- H. Cheng, K. Fuku, Y. Kuwahara, K. Mori and H. Yamashita, *J. Mater. Chem. A*, 2015, **3**, 5244.
- X. Li, J. Zhu and B. Wei, *Chem. Soc. Rev.*, 2016, **45**, 3145.
- P. Lianos, *Appl. Catal., B*, 2017, **210**, 235.
- S. Sahai, A. Ikram, S. Rai, R. Shrivastav, S. Dass and V. R. Satsangi, *Renewable Sustainable Energy Rev.*, 2017, **68**, 19.
- Y. Zhang, S. He, W. Guo, Y. Hu, J. Huang, J. R. Mulcahy and W. D. Wei, *Chem. Rev.*, 2018, **118**, 2927.
- H. Tada, *Dalton Trans.*, 2019, **48**, 6308.
- Y. Tian and T. Tatsuma, *J. Am. Chem. Soc.*, 2005, **127**, 7632.
- A. Furube, L. Du, K. Hara, R. Katoh and M. Tachiya, *J. Am. Chem. Soc.*, 2007, **129**, 14852.
- G. Zhao, H. Kozuka and T. Yoko, *Thin Solid Films*, 1996, **277**, 147.
- K. Awazu, M. Fujimaki, C. Rockstuhl, J. Tominaga, H. Murakami, Y. Ohki, N. Yoshida and T. Watanabe, *J. Am. Chem. Soc.*, 2008, **130**, 1676.
- M. Fujishima, T. Ikeda, R. Akashi and H. Tada, *ACS Omega*, 2018, **3**, 6104.
- R. Asapu, N. Claes, R.-G. Ciocarlan, M. Minjauw, C. Detavernier, P. Cool, S. Bals and S. W. Verbruggen, *ACS Appl. Nano Mater.*, 2019, **2**, 4067.
- K. Ueno, T. Oshikiri and H. Misawa, *ChemPhysChem*, 2016, **17**, 199; N. Wu, *Nanoscale*, 2018, **10**, 2679.
- M. W. Knight, H. Sobhani, P. Norrdlander and N. J. Halas, *Science*, 2011, **332**, 702.
- Y. Hayashido, S. Naya and H. Tada, *J. Phys. Chem. C*, 2016, **120**, 19663.
- Y. Hayashido, S. Naya and H. Tada, *J. Phys. Chem. C*, 2016, **120**, 19663.
- P. Wang, B. Huang, Y. Dai and M.-H. Whangbo, *Phys. Chem. Chem. Phys.*, 2012, **14**, 9813.
- K. H. Leong, A. A. Aziz, L. C. Sim, P. Saravanan, M. Jang and D. Bahnemann, *Beilstein J. Nanotechnol.*, 2018, **9**, 628.
- N. J. Halas and S. Lal, *Chem. Rev.*, 2011, **111**, 3913.
- N. S. Abadeer and C. J. Murphy, *J. Phys. Chem. C*, 2016, **120**, 4691.





- 37 P. K. Jain, X. Huang, I. H. El-Sayed and M. A. El-Sayed, *Acc. Chem. Res.*, 2008, **41**, 1578.
- 38 C. Wang and D. Astruc, *Chem. Soc. Rev.*, 2014, **43**, 7188.
- 39 Y. Shiraishi, Y. Kofuji, H. Sakamoto, S. Tanaka, S. Ichikawa and T. Hirai, *ACS Catal.*, 2015, **5**, 3058.
- 40 Y. Nishijima, K. Ueno, Y. Yokota, K. Murakoshi and H. Misawa, *J. Phys. Chem. Lett.*, 2010, **1**, 2031.
- 41 M. Teranishi, M. Wada, S. Naya and H. Tada, *ChemPhysChem*, 2016, **17**, 2813.
- 42 C. G. Silva, R. Juárez, T. Marino, R. Molinari and H. García, *J. Am. Chem. Soc.*, 2011, **133**, 595.
- 43 L. Liu, P. Li, B. Adisak, S. Ouyang, N. Umezawa, J. Ye, R. Kodiyath, T. Tanabe, G. V. Ramesh, S. Ueda and H. Abe, *J. Mater. Chem. A*, 2014, **2**, 9875.
- 44 R. Negishi, S. Naya, H. Kobayashi and H. Tada, *Angew. Chem., Int. Ed.*, 2017, **56**, 10347.
- 45 R. Sundararaman, P. Narang, A. S. Jermyn, W. A. Goddard III and H. A. Atwater, *Nat. Commun.*, 2014, **5**, 5788.
- 46 B. E. Conway and B. V. Tilak, *Electrochim. Acta*, 2002, **47**, 3571.
- 47 H. Tada, T. Kiyonaga and S. Naya, *Chem. Soc. Rev.*, 2009, **38**, 1849.
- 48 M. Murdoch, G. I. N. Waterhouse, M. A. Nadeem, J. B. Metson, M. A. Keane, R. F. Howe, J. Llorca and H. Idriss, *Nat. Chem.*, 2011, **3**, 489.
- 49 C. M. Sánchez-Sánchez and A. J. Bard, *Anal. Chem.*, 2009, **81**, 8094.
- 50 M. Teranishi, S. Naya and H. Tada, *J. Am. Chem. Soc.*, 2010, **132**, 7850.
- 51 R. Cai, Y. Kubota and A. Fujishima, *J. Catal.*, 2003, **219**, 214.
- 52 H. Goto, Y. Hanada, T. Ohno and M. Matsumura, *J. Catal.*, 2004, **225**, 223.
- 53 T. Hirakawa and Y. Nosaka, *J. Phys. Chem. C*, 2008, **112**, 15818.
- 54 H. Kobayashi, M. Teranishi, R. Negishi, S. Naya and H. Tada, *J. Phys. Chem. Lett.*, 2016, **7**, 5002.
- 55 S. Mubeen, J. Lee, N. Singh, S. Krämer, G. D. Stucky and M. Moskovits, *Nat. Nanotechnol.*, 2015, **8**, 247.
- 56 A. Tanaka, K. Teramura, S. Hosokawa, H. Kominami and T. Tanaka, *Chem. Sci.*, 2017, **8**, 2574.
- 57 N. Buhker, K. Meier and J. F. Reber, *J. Phys. Chem.*, 1984, **88**, 3261.
- 58 H. Tada, T. Mitsui, T. Kiyonaga, T. Akita and K. Tanaka, *Nat. Mater.*, 2006, **5**, 782.
- 59 S. Naya, T. Kume, R. Akashi, M. Fujishima and H. Tada, *J. Am. Chem. Soc.*, 2018, **140**, 1251.
- 60 K. Wu, W. E. Rodríguez-Córdoba, Y. Yang and T. Lian, *Nano Lett.*, 2013, **13**, 5255.
- 61 J. W. Ha, T. P. A. Ruberu, R. Han, B. Dong, J. Vela and N. Fang, *J. Am. Chem. Soc.*, 2014, **136**, 1398.
- 62 K. Takayama, K. Fujiwara, T. Kume, S. Naya and H. Tada, *J. Phys. Chem. Lett.*, 2017, **8**, 86.
- 63 P. Reineck, G. P. Lee, M. Karg, P. Mulvaney and U. Bach, *Adv. Mater.*, 2012, **24**, 4750.
- 64 D. Meissner, R. Memming, B. Kastening and D. Bahnemann, *Chem. Phys. Lett.*, 1986, **127**, 419.
- 65 L. Qin, G. Wang and Y. Tan, *Sci. Rep.*, 2018, **8**, 16198.
- 66 X. Lang, X. Chen and J. Zhao, *Chem. Soc. Rev.*, 2014, **43**, 473; W. Wang and D. Astruc, *Chem. Soc. Rev.*, 2014, **43**, 7188.
- 67 S. Naya, T. Niwa, T. Kume and H. Tada, *Angew. Chem., Int. Ed.*, 2014, **53**, 7305.
- 68 M. Teranishi, R. Hoshino, S. Naya and H. Tada, *Angew. Chem., Int. Ed.*, 2016, **55**, 12773.
- 69 X. Li, C. Chen and J. Zhao, *Langmuir*, 2001, **17**, 4118.
- 70 C. Minero, G. Mariella, V. Maurino and E. Pelizzetti, *Langmuir*, 2000, **16**, 2632.
- 71 H. Park and W. Choi, *J. Phys. Chem. B*, 2004, **108**, 4086.
- 72 V. Maurino, C. Minero, G. Mariella and E. Pelizzetti, *Chem. Commun.*, 2005, 2627.
- 73 Y. Shiraishi, S. Kanazawa, Y. Kofuji, H. Sakamoto, S. Ichikawa, S. Tanaka and T. Hirai, *Angew. Chem., Int. Ed.*, 2014, **53**, 13454.
- 74 S. Siahrostami, A. Verdager-Casadevall, M. Karamad, D. Deiana, P. Malacrida, B. Wickman, M. Escudero-Escribano, E. A. Paoli, R. Frydendal, T. W. Hansen, I. Chorkendorff, I. E. L. Stephens and J. Rossmeisl, *Nat. Mater.*, 2013, **12**, 1137.
- 75 R. S. Moakhar, M. Jalali, A. Kushwaha, G. K. L. Goh, N. Riahi-Noori, A. Dolati and M. Ghorbani, *J. Appl. Electrochem.*, 2018, **48**, 995.
- 76 W. Shi, C. Ma, H. Wang, D. Duan, Z. Sun and S. Yang, *Int. J. Hydrogen Energy*, 2018, **43**, 18850.
- 77 A. Malankowska, M. P. Kobylański, A. Mikolajczyk, O. Cavdar, G. Nowaczyk, M. Jarek, W. Lisowski, M. Michalska, E. Kowalska, B. Ohtani and A. Zaleska-Medynska, *ACS Sustainable Chem. Eng.*, 2018, **6**, 16665.
- 78 K. Kitazono, R. Akashi, K. Fujiwara, A. Akita, S. Naya, M. Fujishima and H. Tada, *ChemPhysChem*, 2017, **18**, 2840.
- 79 K. Awa, R. Akashi, A. Akita, S. Naya, H. Kobayashi and H. Tada, *ChemPhysChem*, 2019, **20**, 2155.
- 80 L. Wen, R. Xu, C. Cui, W. Tang, Y. Mi, X. Lu, Z. Zeng, S. L. Suib, P.-X. Gao and Y. Lei, *Nano Lett.*, 2018, **18**, 4914.
- 81 C. Marchal, T. Cottineau, M. G. Méndez-Medrano, C. Colbeau-Justin, V. Caps and V. Keller, *Adv. Energy Mater.*, 2018, 1702142.
- 82 D. A. Panayotov and J. R. Morris, *Surf. Sci. Rep.*, 2016, **71**, 77.

